Supporting Information

Metal-Organic-Framework Approach to Engineer Hollow Bimetal Oxide Microspheres towards Enhanced Electrochemical Performances of Lithium Storage

Weiwei Sun†*, Si Chen*†*, Yong Wang**

Department of Chemical Engineering, School of Environmental and Chemical Engineering, Shanghai University, 99 Shangda Road, Shanghai, P. R. China, 200444
Corresponding authors: Tel: +86-21-66137723; Fax: +86-21-66137725;
Email address: yongwang@shu.edu.cn (Y. Wang)

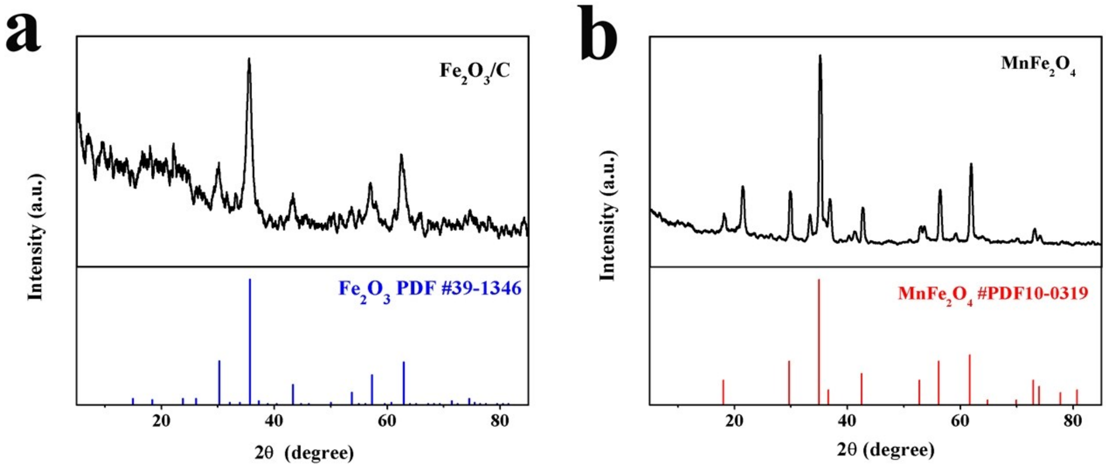

Fig. S1 XRD patterns of the benchmarked products: (a) Fe_2O_3/C and (b) $MnFe_2O_4$. The characteristic peaks in the XRD patterns of Fe_2O_3/C and $MnFe_2O_4$ are in good accordance with the standard Fe_2O_3 (PDF Card No.39-1346) and $MnFe_2O_4$ (PDF Card No.10-0319).

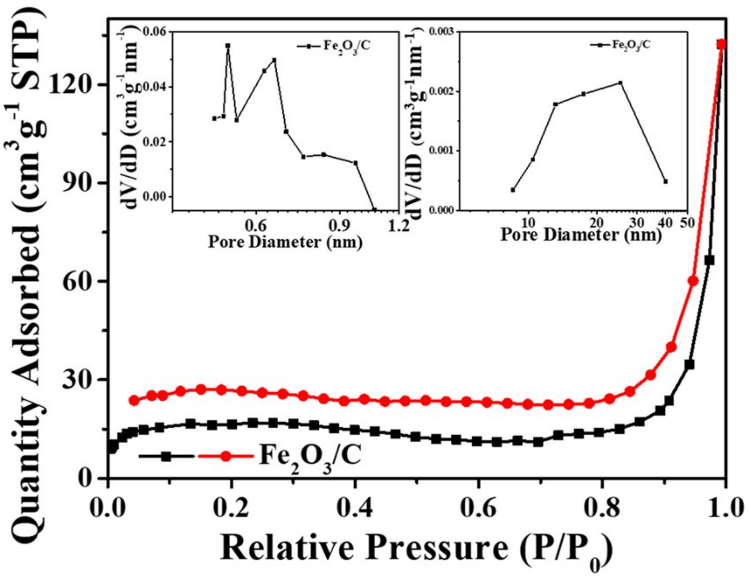

Fig. S2 N_2 adsorption/desorption isothermal curves and the pore distribution (the insert) of Fe_2O_3/C composite. The specific surface area of ~55.4 m^2 g^{-1} can be detected with the existence of mesopores (pore size centered at ~12-27 nm) and micropores (pore size centered at ~0.4-1.0 nm).

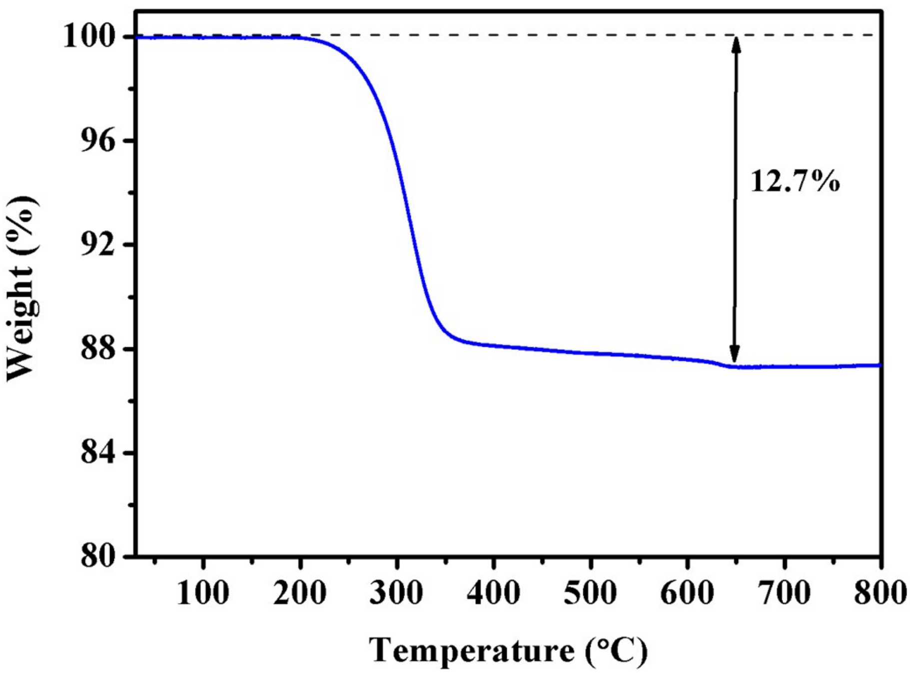

Fig. S3 TGA curve of Fe-Mn-O/C in air atmosphere. The weight loss of 12.7 % between 200-700 °C should be assigned to the oxidation of carbon, indicating 12.7 % carbon in the Fe-Mn-O/C composite.

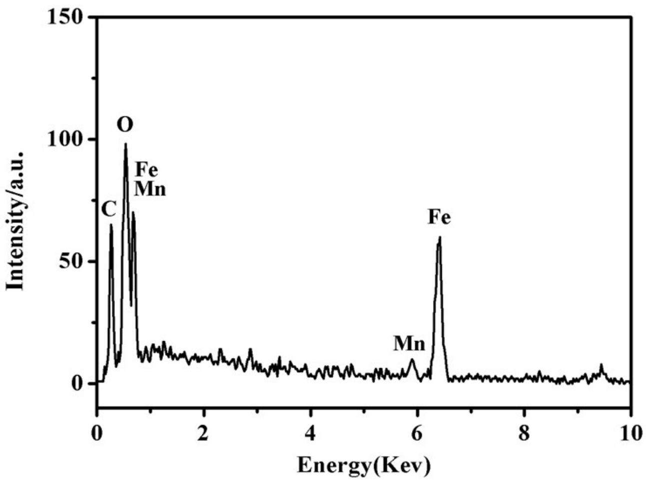

Fig. S4 EDS spectrum of Fe-Mn-O/C. Four elements of Fe, Mn, O, and C can be detected with the molar ratios being 9:1:15:10. The content of C in the Fe-Mn-O/C composite can also be detected to be 12.6 %.

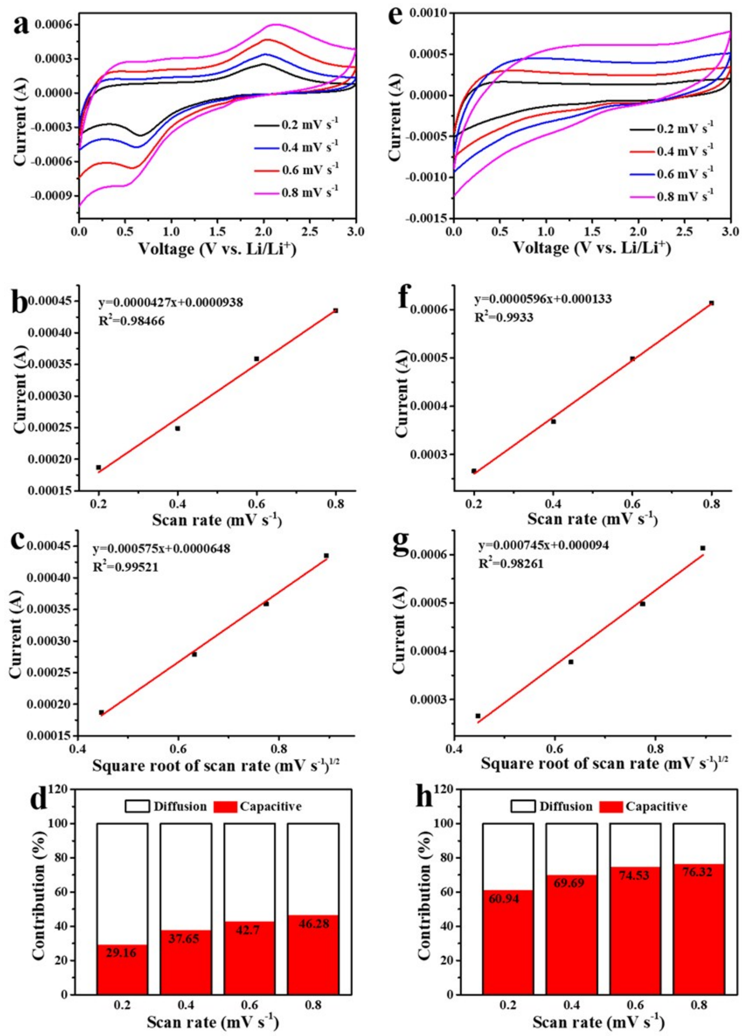

Fig. S5 (a) CV curves of the as-synthesized Fe_2O_3/C electrode with different scan rates of 0.2, 0.4, 0.6, and 0.8 mV s^{-1}. The linear fit of (b) peak currents vs. scan rate and (c) peak currents vs. square root of scan rate for the as-synthesized Fe_2O_3/C electrode. (d) Contribution ratio of capacitive and diffusion-controlled behaviors at different scan rates of as-prepared Fe_2O_3/C electrode. (e) CV curves of the cycled Fe_2O_3/C electrode after 200 cycles with different scan rates of 0.2, 0.4, 0.6, and 0.8 mV s^{-1}. The linear fit of (f) peak currents vs. scan rate and (g) peak currents vs. square root of scan rate for the cycled Fe_2O_3/C electrode after 200 cycles. (h) Contribution ratio of capacitive and diffusion-controlled behaviors at different scan rates of cycled Fe_2O_3/C electrode after 200 cycles.

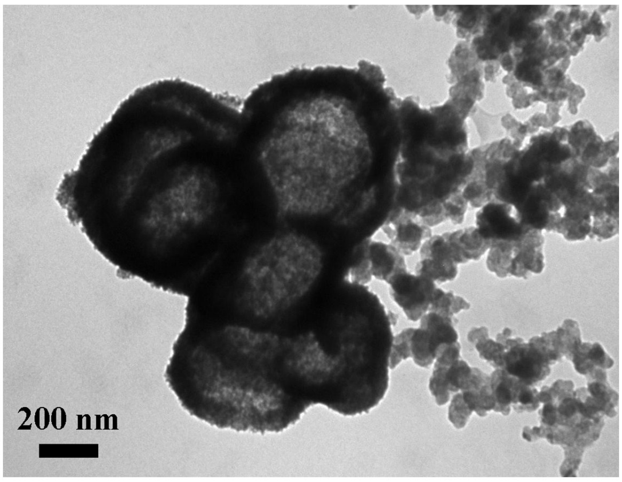

Fig. S6 TEM image of the Fe-Mn-O/C electrode after 200 cycles. The sustainably retained hollow nanosphere morphology of the Fe-Mn-O/C electrode can be detected after cycling.

Table S1 Electrochemical properties of Fe-Mn-O/C of this work and previous related work derived from MOFs. (IRC: initial reversible capacity, mA h g^{-1}; RRC: retained reversible capacity, mA h g^{-1}; CN: cycle number; CD: current density, A g^{-1}; V: voltage, V)

Composite	Morphology	IRC	RRC/CN	CD	V	References
Fe_2O_3-Mn_3O_4-C	Hollow nanosphere	837	1294/200	0.1	0.005-3.0	This work
Fe_2O_3	Nanocube	~850	~800/50	0.2	0.05-3.0	1
Fe_2O_3	Microbox	917	~630/30	0.2	0.05-3.0	2
Fe_2O_3	Nanospindle	~1024	~920/40	0.1	0.005-3.0	3
Fe_2O_3	Hierarchical microbox	~945	~920/30	0.2	0.01-3.0	4
Fe_2O_3	Nanospindle	940	911/50	0.2	0.01-3.0	5
Fe_2O_3	Yolk-shell octahedron	1060	1176/200	0.1	0.005-3.0	6
Fe_2O_3	Microcube	~1420	~608/50	0.1	0.05-3.0	7
Fe_2O_3@N-doped C	Hollow nanosphere	1368	1573/50	0.1	0.01-3.0	8
Fe_2O_3/graphene	Nanoparticle in graphene aerogel	~1174	1129/130	0.2	0.01-3.0	9
Fe_2O_3@graphene	Hollow nanosphere	~950	~833/100	1	0.01-3.0	10
Mn_3O_4/C	Sponge network	722	770/100	0.2	0.005-2.5	11
Mn_3O_4/C	Microsphere	1205	1032/500	0.2	0.01-3.0	12

References:

1 L. Zhang, H. B. Wu, R. Xu, and X. W. Lou, *CrystEngComm*, 2013, **15**, 9332-9335..

2 L. Zhang, H. B. Wu, and X. W. Lou, *J. Am. Chem. Soc.*, 2013, **135**, 10664-10672.

3 A. Banerjee, V. Aravindan, S. Bhatnagar, D. Mhamane, S. Madhavi and S. Ogale, *Nano Energy*, 2013, **2**, 890-896.

4 L. Zhang, H. B. Wu, S. Madhavi, H. H. Hng, and X. W. Lou, *J. Am. Chem. Soc.*, 2012, **134**, 17388-17391.

5 X. Xu, R. Cao, S. Jeong, and J. Cho, *Nano Lett*, 2012, **12**, 4988-4991..

6 W. X. Guo, W. W. Sun, L. P. Lv, S. F. Kong, and Y. Wang, *ACS Nano*, 2017, **11**, 4198-4205.

7 M. Li, W. Wang, M. Yang, F. Lv, L. Cao, Y. Tang, R. Sun, and Z. Lu, *RSC Adv.*, 2015, **5**,7356-7362.

8 F. Zheng, M. He, Y. Yang, and Q. Chen, *Nanoscale*, 2015, **7**, 3410-3417.

9 T. Jiang, F. Bu, X. Feng, I. Shakir, G. Hao, and Y. Xu, *ACS Nano*, 2017, **11**, 5140-5147.

10 J. Hu, J. Zheng, L. Tian, Y. Duan, L. Lin, S. Cui, H. Peng, T. Liu, H. Guo, X. Wang, and F. Pan, *Chem. Commun.*, 2015, **51**, 7855-7858.

11 B. Sambandam, V. Soundharrajan, J. J. Song, S. Kim, J. Jo, D. P. Tung, S. Kim, V. Mathew, and J. Kim, *Inorg. Chem. Front.*, 2016, **3**, 1609-1615.

12 H. J. Peng, G. X. Hao, Z. H. Chu, J. Lin, X. M. Lin, and Y. P. Cai, *Cryst. Growth Des.*, 2017, **17**, 5881-5886.